A

```
                β-hairpin          Helix1              Helix2        Helix3      Helix4
NL4-3   1 PIVQNLQGQMVHQAISPRTLNAWVKVVEEKAFSPEVIPMFSALSEGATPQDLNTMLNTVGGHQAAMQMLK 70
LNEIE   1 .........L.............................................................. 70
LSDQ    1 .............................................................................. 70
MA239   1 .-..QIG.NY..LPL.........LI...K.GA..V.G.Q.....C..Y.I.Q...C..D......IIR 69

                Helix4      CypA binding loop      Helix5      Helix6          Helix7
NL4-3  71 ETINEEAAEWDRLHPVHAGPIAPGQMREPRGSDIAGTTSTLQEQIGWMTHNP-PIPVGEIYKRWIILGLN 139
LNEIE  71 ..................NE...I..................E......-................. 139
LSDQ   71 ..............QP.-.QQ-..L...S..........D...Q...RQQN................. 138
MA239  70 DI......D..LQ..QP.-.QQ-..L...S.........SVD...Q..YRQQN.....N..R...Q...Q 137
```

B

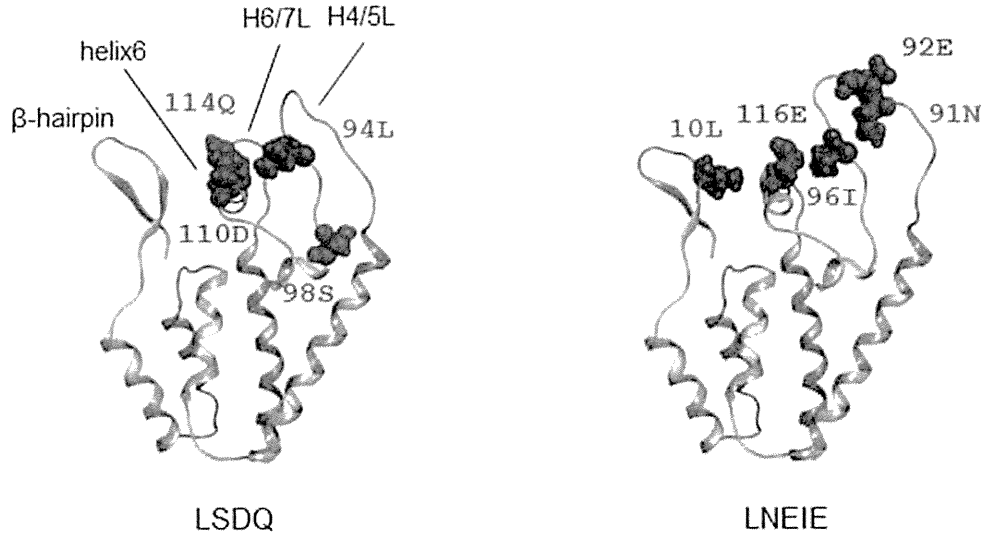

C

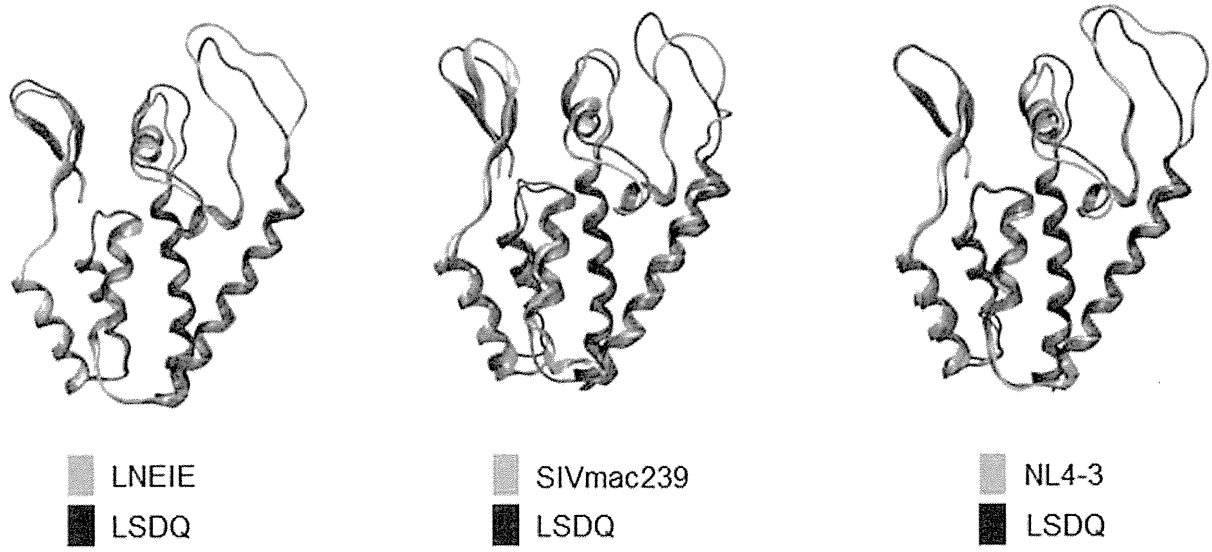

Fig. 1. Structure of CA NTD from two different HIV-1mt clones. (A) Alignment of CA sequences. Amino acid sequences in CA (amino acid residues 1 to 137/138/139) of HIV-1_{NL4-3} (GenBank: AF324493), LNEIE [16], LSDQ [15], and SIVmac239 (GenBank: M33262) were aligned by Genetix ver. 11. Dots show the same amino acid residues with those of HIV-1_{NL4-3}. Hyphens indicate the gap. The domains of β-hairpin and helices 1 to 7 are indicated based on the previous publication [37]. (B) Structural models for CA NTD from two distinct HIV-1mt clones LSDQ and LNEIE. Molecular models were constructed by homology modeling and were refined as previously described [15]. HIV-1 CA NTD at a resolution of 1.95Å (PDB code: 4LQW) [20] was used as modeling template. (C) Superimposition of the CA structures. Superposed structures of LNEIE/LSDQ CAs (left), SIVmac239 (modified structure of PDB code 4HTW)/LSDQ CAs (middle), and NL4-3 (PDB code 3GV2)/LSDQ CAs (right) are shown using two different colors indicated.

mononuclear cells (PBMCs) among the macaque-tropic HIV-1 (HIV-1mt) clones examined in each study [15,16]. In this work, we aimed to gain virological and structural insights into evasion from TRIM5α-restriction using the two distinct HIV-1 CAs.

2. Materials and methods

2.1. Plasmid DNA

An HIV-1mt clone designated MN4/LSDQgtu and a standard SIVmac clone designated SIVmac239 used in this study were described previously [15]. Clone pLNEIE was constructed by introduction of the five mutations [16] into the CA-coding region of a sub-genomic clone derived from pNL4-3 by QuickChange Site-Directed Mutagenesis kit (Agilent Technologies Inc., Santa Clara, CA). Clone pSCA was constructed from the above sub-genomic clone by overlapping PCR and QuickChange Site-Directed Mutagenesis kit to have Gag sequences as described for stHIV-1_{SCA} [16,17]. Proviral clones designated LSDQ+4gtu, LNEIE+4gtu, and SCA+4gtu were generated by replacement of the *Bss*HII-*Sbf*I DNA fragment of MN4/LSDQgtu with the corresponding fragments of "MN4/LSDQgtu", pLNEIE, and pSCA clones, respectively.

2.2. Cell culture, virus preparation, and reverse transcriptase (RT) assays

A human kidney cell line 293T, a RhM lymphocytic cell line M1.3S and RhM PBMCs were cultured as described previously [15]. The *TRIM5* genotypes of PBMCs, prepared from RhM individuals and used for infection experiments, were determined as described previously [15]. Virus stocks were prepared from 293T cells transfected with proviral clones on day 2 post-transfection. Virus stocks were assayed for RT activities, and used for infection experiments as previously described [15].

2.3. TRIM5 susceptibility assays

TRIM5 susceptibility assays in human MT4 cells were done by the recombinant Sendai virus (SeV)-TRIM5 expression system as described previously [15,18].

2.4. Multi-cycle virus replication assays

Infection of M1.3S cells was ordinarily performed as described previously [15]. For infection of RhM PBMCs, the spinoculation method [19] was used. Virus replication was monitored by RT activity released into the culture supernatants.

2.5. Structural analysis

Molecular models for HIV-1mt CA N-terminal domain (NTD) were constructed by homology modeling and were refined as described previously [15]. HIV-1 CA NTD at a resolution of 1.95Å (PDB code: 4LQW) [20] was used as modeling template. Superimpositions of the structures were done using the Protein Superpose module in MOE (Chemical Computing Group Inc., Quebec, Canada).

3. Results

3.1. Sequence and structure comparison of LSDQ and LNEIE CAs

Determinants in retroviral CA to modulate TRIM5α-susceptibility have been mapped to CA surface domains including β-hairpin, a loop between helices 4 and 5 (H4/5L), helix6, and H6/7L (Fig. 1A) [15,18,21–29]. LSDQ and LNEIE, the two RhM TRIM5α-resistant HIV-1 CAs, have different amino acid sequences, convergently in a cyclophillin A (CypA) binding loop within H4/5L and in H6/7L. The loop regions in LSDQ CA have been replaced with those in SIVmac239 CA (Fig. 1A). As indicated in Fig. 1B, LSDQ and LNEIE CAs commonly gained a negatively charged amino acid residue in helix6 (110D for LSDQ and 116E for LNEIE) and paired substitutions in helix6 and H4/5L (114Q/94L for LSDQ and 116E/96I for LNEIE). However, the overall appearance of CA NTD was different between the two clones mainly due to difference in H4/5L- and H6/7L-length, which could affect a surface pattern of viral core (Fig. 1C, left). In addition, the structure of LSDQ CA was different from those of its parental CAs, i.e., SIVmac239 and NL4-3 CAs, especially in the H4/5L region (Fig. 1C, middle and right). Moreover, the β-hairpin domain of SIVmac239 CA was structurally distinct from those of LSDQ, LNEIE, and NL4-3 CAs (Fig. 1C). Conclusively, LSDQ and LNEIE CAs are structurally unique to each other (Fig. 1), but both contribute to the TRIM5α-resistance [15,16].

3.2. LSDQ and LNEIE CAs exhibit different susceptibilities to the restriction mediated by various macaque TRIM5 proteins

To examine potentials of the two distinct CAs for evading TRIM5α-restriction and for viral replication, we constructed new proviral clones in the backbone of our best HIV-1mt designated MN4/LSDQgtu (Fig. 2A) [15]. The *Bss*HII-*Sbf*I DNA fragment of MN4/LSDQgtu was replaced with the corresponding fragments of LNEIE [16] and LSDQ [15] to generate LNEIE+4gtu and LSDQ+4gtu, respectively. The sequence differences between the two clones reside only in the CA NTD (Fig. 1A).

First, we determined susceptibility of LSDQ+4gtu and LNEIE+4gtu to various TRIM5 proteins expressed by SeV vectors. Ability of viral clones to evade TRIM5-restriction, in comparison with that of SIVmac239, can be readily determined by this recombinant SeV-TRIM5 overexpression system [15,18]. Macaque TRIM5 alleles are divided into three functionally different groups: $TRIM5\alpha^{TFP}$, $TRIM5\alpha^{Q}$, and $TRIM5^{CypA}$ [30–32]. TRIM5α proteins of both RhM and cynomolgus macaque (CyM), and CyM TRIM5CypA inhibit HIV-1 replication, but not RhM TRIM5CypA [33,34]. Thus,

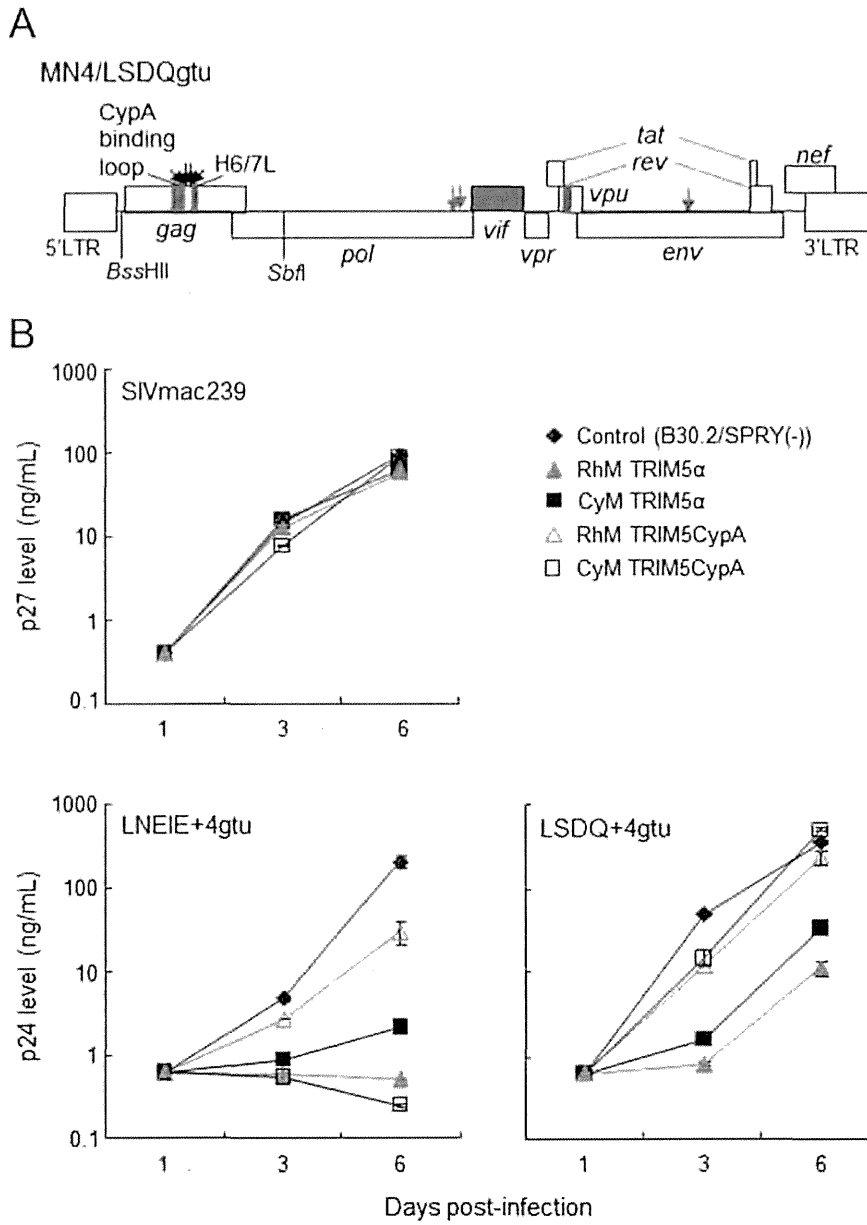

Fig. 2. Susceptibility of viral clones to various macaque TRIM5 proteins. (A) Proviral genome structure of an HIV-1mt clone MN4/LSDQgtu [15]. Blue and red areas show sequences from SIVmac239 and SIVgsn166 (SIV isolated from the greater spot-nosed monkey) (GenBank: AF468659), respectively. Green arrows show the adaptive mutations that enhance the viral growth potential [38]. Four amino acid substitutions (M94L/R98S/Q110D/G114Q) in CA that increase RhM TRIM5α-resistance are indicated by black arrows [15]. The *Bss*HII and *Sbf*I sites used for construction of MN4/LSDQgtu-based viral clones carrying distinct CAs are indicated. (B) TRIM5 susceptibility assays. Human MT4 cells (1.0×10^5) were infected with recombinant SeV expressing B30.2/SPRY (−) TRIM5, CyM TRIM5α (*TRIM5α*^{Q}), RhM TRIM5α (*TRIM5α*^{TFP}), CyM TRIM5CypA (*TRIM5*^{CypA}), or RhM TRIM5CypA (*TRIM5*^{CypA}). B30.2/SPRY (−) TRIM5 without the ability to restrict viral replication served as a control. Nine hours after infection with recombinant SeVs, cells were super-infected with 20 ng (Gag-p24) of HIV-1mt clones or 20 ng (Gag-p27) of SIVmac239. Virus replication was monitored by the amount of Gag-p24 (HIV-1mt clones) or Gag-p27 (SIVmac239) in the culture supernatants. Error bars show fluctuations between duplicate samples. Representative data from two independent experiments are shown. (For interpretation of the references to color in this figure legend, the reader is referred to the web version of this article.)

we tested here four different TRIM5 alleles, i.e., RhM TRIM5α (*TRIM5α*^{TFP}), CyM TRIM5α (*TRIM5α*^{Q}), RhM TRIM5CypA (*TRIM5*^{CypA}), and CyM TRIM5CypA (*TRIM5*^{CypA}), using B30.2/SPRY(−) TRIM5 as a control. As shown in Fig. 2B, SIVmac239 replicated similarly well in the presence of RhM TRIM5α, CyM TRIM5α, RhM TRIM5-CypA, or CyM TRIM5CypA as in control cells expressing B30.2/SPRY(−) TRIM5. While not complete as compared with the case of SIVmac239 [15], LSDQ+4gtu showed more resistance to various RhM/CyM TRIM5 proteins than LNEIE+4gtu. In particular, consistent with previous observations, LSDQ+4gtu replicated well in the presence of CyM TRIMCypA, but not at all LNEIE+4gtu [15,16]. Furthermore, in the presence CyM/RhM TRIM5α, LNEIE+4gtu appeared to replicate (note the data in the presence of CyM TRIM5-CypA in Fig. 2B) but clearly more poorly than LSDQ+4gtu.

Table 1
Lethal mutations in CA of MN4/LSDQgtu.[a]

Mutants	CA mutations relative to LSDQ	CA domains	References
P37S-LSDQ	P38S	Helix2	[35]
LSVDQ	L109V	Helix6	[25]
LSDQY	T117Y	Helix6	
LSVDQY	L109V/T117Y	Helix6	
Mutants of β-hairpin domain	Amino acid sequences in β-hairpin[b]		
LSDQ (parental clone)	PIVQNLQGQMVHQAI		[15]
Wild-type SIVmac239	PVQQIGGNYVHLPL		
M10L-LSDQ	PIVQNLQGQ**L**VHQAI		[16]
Q13L-LSDQ	PIVQNLQGQMVH**L**AI		
IGGN-LSDQ	PIVQ**IGGN**MVHQAI		
Beta-1	P**VQ**Q**IGGN**MVHQAI		
Beta-2	PIVQ**IGGNY**VH**L**AI		
Beta-3	PIVQNLQGQMVH**LPL**		
Beta-4	P**VQ**QNLQGQMVHQAI		
Beta-5	PIVQ**IGGNY**VHQAI		
Beta-6	P**VQ**Q**IGGNY**VH**L**AI		
Beta-7	P**VQ**Q**IGGNY**VH**LPL**		
Beta-8	PIVQ**IGGNY**VH**LPL**		

[a] Lethal mutations as judged by viral replication in M1.3S cells during the observation period (15 days).
[b] Bold letters show the mutations introduced into LSDQ CA. For alignment of four CA NTD sequences, see Fig. 1A.

These results show that LSDQ and LNEIE have intrinsically different abilities to negotiate anti-viral effects of various macaque TRIM5 proteins.

Amino acid substitutions in CA contributing to escape from RhM TRIM5α-restriction have been identified by *in vivo* adaptation of SIVsm (SIV from the sooty mangabey) in RhM (P37S and R97S in SIVsm CA) [30,35], and by "gain-of-sensitivity assays" using SIVmac239 CA (L93M, S97R, V108L, D109Q, and Q113G) [25]. TRIM5-resistant LSDQ CA already has M94L, R98S, Q110D, and G114Q mutations corresponding to L93, S97, D109, and Q113 residues in SIVmac239 CA [15]. Therefore, it was possible that amino acid substitutions such as P38S (corresponding to P37S in SIVsm and SIVmac239 CAs) and L109V (corresponding to V108 in SIVmac239 CA) in LSDQ CA might enhance its TRIM5-resistance. The β-hairpin domain in retroviral CAs is also an important determinant for evasion from TRIM5α-restriction [18,25,27] (Fig. 1C). Based on these considerations, we introduced various amino acid substitutions into the MN4/LSDQgtu CA (Table 1) to increase TRIM5α-resistance, hopefully up to the SIVmac239 CA level. Resultant proviral clones were tested for their growth abilities in a RhM cell line M1.3S. However, our extensive attempts to obtain biologically active CAs, potentially more resistant to macaque TRIM5 proteins than MN4/LSDQgtu CA, were unsuccessful so far (Table 1). Thus, some mutation(s) and/or combination(s) of mutations in CA other than those in Table 1 may be necessary to confer full resistance to TRIM5α on the HIV-1mt.

3.3. HIV-1mt clones carrying LSDQ/LNEIE CA replicate well in RhM PBMCs

To compare the effects of a different spectrum of mutations in CAs on viral growth potential, we examined LSDQ+4gtu and LNEIE+4gtu for their replication in RhM cells. In M1.3S cells (*TRIM5α$^{TFP/TFP}$*) [36], LSDQ+4gtu replicated slightly better than LNEIE+4gtu (Fig. 3A). In PBMCs prepared from four RhM individuals (*TRIM5α$^{TFP/Q}$*), LSDQ+4gtu grew better (Fig. 3B, upper panel) than or similarly to LNEIE+4gtu (Fig. 3B, lower panel). Next, to compare the competence of the CAs to that of SIVmac239 CA in terms of multi-cycle virus replication in RhM PBMCs, we newly constructed a proviral HIV-1mt clone carrying SIVmac239 CA. Because insertion of the entire CA-coding sequence of SIVmac into the corresponding region of HIV-1 genome was lethal, we generated a new Gag clone (SCA) exactly as previously reported for stHIV-1$_{SCA}$ [16,17] (Fig. 4A), and then made a proviral clone designated SCA+4gtu as described to construct LSDQ+4gtu and LNEIE+4gtu (Fig. 2A) for infection experiments. Proviral clone SCA was more replication-competent than LSDQ [15] (~3-fold) as determined in feline CRFK cells stably expressing RhM-TRIM5α (*TRIM5α$^{TFP/TFP}$*), but showed a lower titer (~2-fold–4-fold) in CRFK-naïve cells and TZM-bl indicator cells relative to LSDQ (our unpublished results). As shown in Fig. 4B, while LSDQ+4gtu grew better than SCA+4gtu in all four PBMC preparations tested (*TRIM5α$^{TFP/Q}$*), LNEIE+4gtu did so in two preparations (PBMCs from RhMs 610 and 611). In these two PBMC preparations, LSDQ+4gtu and LNEIE+4gtu grew similarly well. In the other two preparations, of note, LSDQ+4gtu grew better than LNEIE+4gtu (PBMCs from RhMs 599 and 609 in Fig. 4B). It remains to be elusive whether the observed difference in growth potentials in some PBMC preparations of the two clones are attributable to TRIM5α-restriction, viral fitness (infectivity of LNEIE determined in TZM-bl indicator cells relative to that of LSDQ was 0.72 on average), unknown cellular factor(s), and/or cellular physiological state/environments.

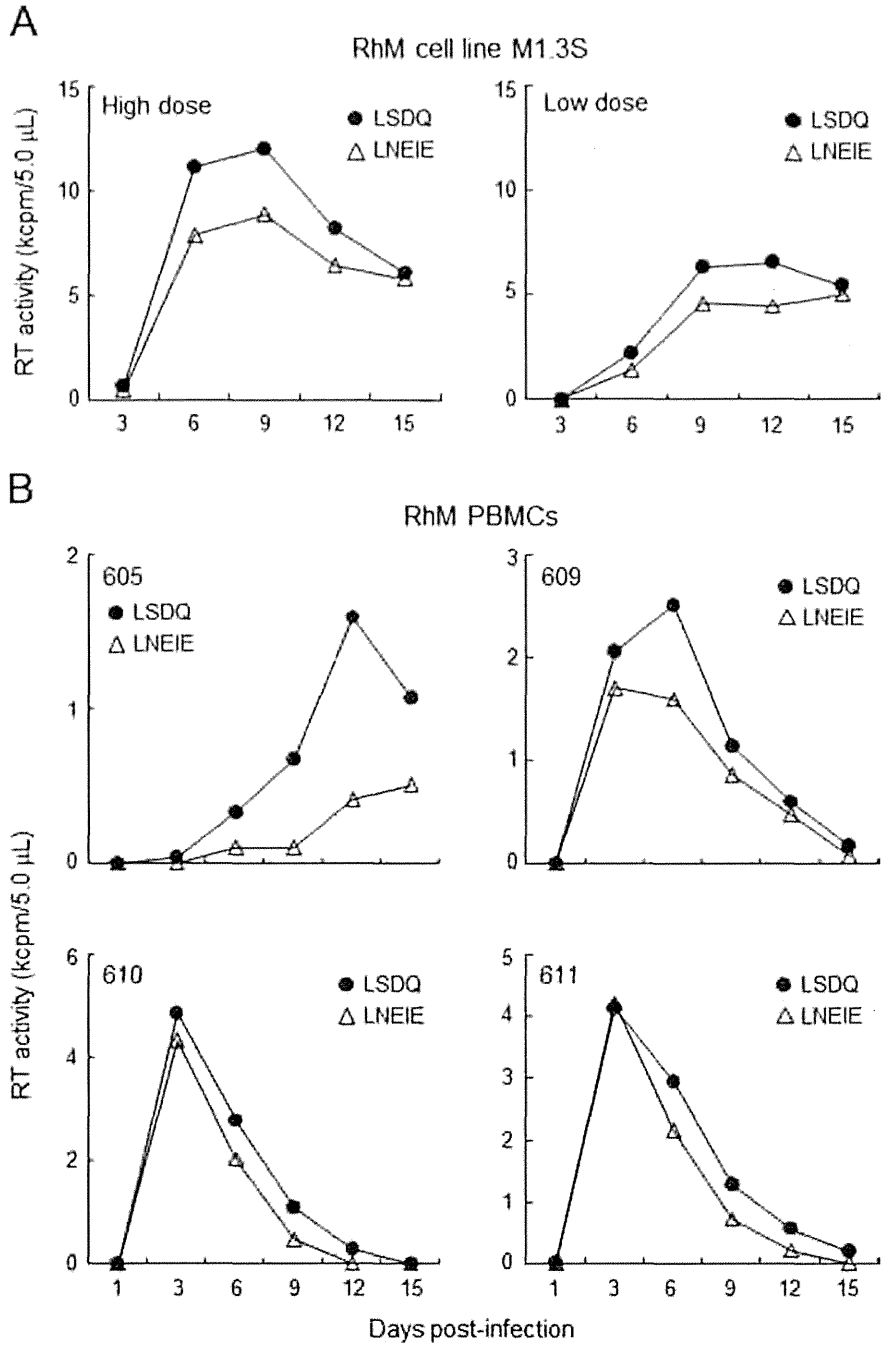

Fig. 3. Growth kinetics of two HIV-1mt clones with a distinct CA in RhM cells. Input viruses were prepared from 293T cells transfected with the indicated clones, and viral replication was monitored by RT activity released into the culture supernatants. LSDQ, LSDQ+4gtu; LNEIE, LNEIE+4gtu. (A) Infection of M1.3S cells (*TRIM5α*$^{TFP/TFP}$). Cells (2.0×10^5) were infected with equal virus amounts (High dose, 5.0×10^5 RT units; Low dose, 5.0×10^4 RT units). (B) Infection of PBMCs from four RhM individuals (*TRIM5α*$^{TFP/Q}$). Equal amounts of viruses were spin-infected into the PBMC preparations. Infection conditions were as follows: 2.4×10^6 RT units/1.0×10^6 cells for monkey 605; 4.0×10^6 RT units/2.0×10^6 cells for monkeys 609, 610, and 611.

4. Discussion

In this study, we performed side by side comparative analyses of the TRIM5-resistance/growth ability in RhM cells of HIV-1mt viruses carrying distinct CAs (LSDQ and LNEIE in Fig. 1) that are resistant to RhM TRIM5α [15,16]. LSDQ and LNEIE CAs exhibited various degrees of susceptibility to macaque TRIM5 proteins, and the former was generally more resistant to TRIM5-restriction than the latter in our TRIM5-overexpression system (Fig. 2). However, growth potentials of HIV-1mt viruses carrying LSDQ or LNEIE CA were similar in some preparations of RhM PBMCs, and varied among PBMCs from RhM individuals with *TRIM5*$^{TFP/Q}$ (Figs. 3 and 4). These results may only reflect a low endogenous expression level of TRIM5 proteins in PBMCs relative to that in cells infected with recombinant SeVs. The expression levels of TRIM5 proteins in various cells, however, can not be measured as yet due to the lack of appropriate anti-macaque

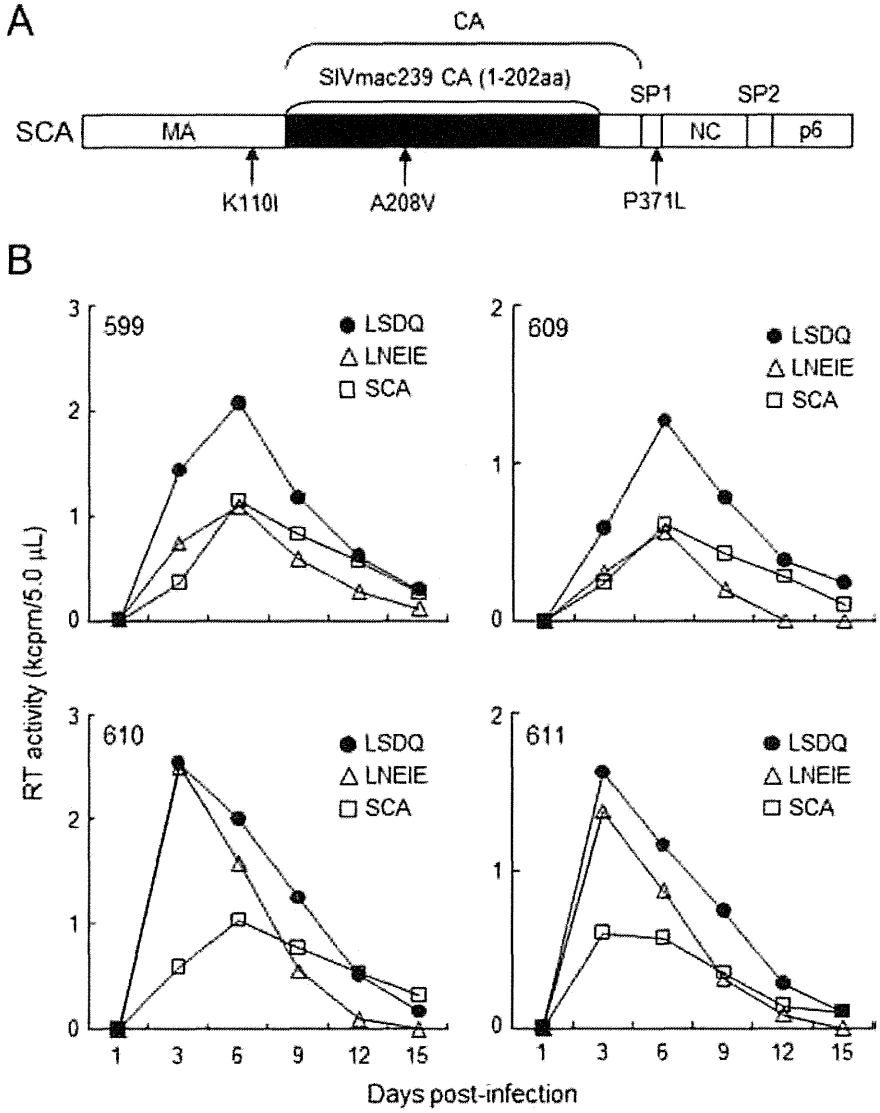

Fig. 4. Growth kinetics of various HIV-1mt clones with a distinct CA in RhM PBMCs. (A) Gag-coding region of pSCA. White and black areas show sequences from HIV-1_{NL4-3} and SIVmac239, respectively. Mutations introduced are indicated. MA, matrix; SP1, spacer peptide 1; NC, nucleocapsid; SP2, spacer peptide 2. (B) Infection of PBMCs from four RhM individuals (*TRIM5α*$^{TFP/Q}$). Input viruses were prepared from 293T cells transfected with the indicated clones, and equal amounts of viruses were spin-infected into the PBMCs. Infection conditions were as follows: 2.4 × 10^6 RT units/2.0 × 10^6 cells for monkey 599; 1.2 × 10^6 RT units/1.0 × 10^6 cells for monkeys 609, 610, and 611. Viral replication was monitored by RT activity released into the culture supernatants. LSDQ, LSDQ+4gtu; LNEIE, LNEIE+4gtu; SCA, SCA+4gtu.

TRIM5 antibodies. Alternatively, the above results suggest that overcoming TRIM5-restriction may not be enough for maximal virus growth of the HIV-1mt clones in RhM cells. Thus, a new generation of HIV-1mt clones that replicate constantly well in PBMCs from any RhM individuals like SIVmac239 would be necessary to establish the HIV-1-infected RhM model system. Of similar importance, detailed biological and structural analyses of the interaction between LSDQ/LNEIE CA and macaque TRIM5 proteins would contribute to better understand the underlying molecular mechanism for HIV-1 restriction by the proteins.

We previously suggested that R98S in HIV-1mt CA may be a key residue to circumvent macaque TRIM5α-restriction [15], since the corresponding residues in SIVsm and SIVmac239 CAs have been shown to contribute to the alteration of TRIM5α-susceptibility [25,30,35]. The coincidence of four amino acid residues important for evasion of RhM TRIM5-restriction in two independent studies on HIV-1 [15] and SIV [25] (L93, S97, D109, Q113 for SIVmac239 CA and L94, S98, D110, Q114 for HIV-1mt CA as described above) has raised a possible involvement of some specific amino acids in the TRIM5-regulation. However, comparative analysis of LSDQ and LNEIE clones here suggests that combinations of mutations in an appropriate context in CA rather than individual residues are critical for efficient escape from TRIM5α-restriction. As TRIM5α has evolved to target diverse retroviral CAs by flexibility of its B30.2/SPRY domain [7-9,12], HIV-1 can, in turn, gain RhM TRIM5α-resistance

through several distinct CAs with different amino acid sequences and/or CA surface patterns.

Conflict of interest

The authors declare that they have no conflict of interest.

Acknowledgments

We thank Ms. Kazuko Yoshida for editorial assistance. This study was supported in part by a grant from the Ministry of Health, Labor and Welfare of Japan (Research on HIV/AIDS project no. H24-005).

References

[1] Kratovac Z, Virgen CA, Bibollet-Ruche F, Hahn BH, Bieniasz PD, Hatziioannou T. Primate lentivirus capsid sensitivity to TRIM5 proteins. J Virol 2008;82:6772–7.

[2] Perron MJ, Stremlau M, Song B, Ulm W, Mulligan RC, Sodroski J. TRIM5alpha mediates the postentry block to N-tropic murine leukemia viruses in human cells. Proc Natl Acad Sci U S A 2004;101:11827–32.

[3] Song B, Javanbakht H, Perron M, Park DH, Stremlau M, Sodroski J. Retrovirus restriction by TRIM5alpha variants from old world and new world primates. J Virol 2005;79:3930–7.

[4] Stremlau M, Owens CM, Perron MJ, Kiessling M, Autissier P, Sodroski J. The cytoplasmic body component TRIM5alpha restricts HIV-1 infection in old world monkeys. Nature 2004;427:848–53.

[5] Yap MW, Nisole S, Lynch C, Stoye JP. Trim5alpha protein restricts both HIV-1 and murine leukemia virus. Proc Natl Acad Sci U S A 2004;101:10786–91.

[6] Ylinen LM, Keckesova Z, Wilson SJ, Ranasinghe S, Towers GJ. Differential restriction of human immunodeficiency virus type 2 and simian immunodeficiency virus SIVmac by TRIM5alpha alleles. J Virol 2005;79:11580–7.

[7] Biris N, Tomashevski A, Bhattacharya A, Diaz-Griffero F, Ivanov DN. Rhesus monkey TRIM5α SPRY domain recognizes multiple epitopes that span several capsid monomers on the surface of the HIV-1 mature viral core. J Mol Biol 2013;425:5032–44.

[8] Biris N, Yang Y, Taylor AB, Tomashevski A, Guo M, Hart PJ, et al. Structure of the rhesus monkey TRIM5α PRYSPRY domain, the HIV capsid recognition module. Proc Natl Acad Sci U S A 2012;109:13278–83.

[9] Ganser-Pornillos BK, Chandrasekaran V, Pornillos O, Sodroski JG, Sundquist WI, Yeager M. Hexagonal assembly of a restricting TRIM5α protein. Proc Natl Acad Sci U S A 2011;108:534–9.

[10] Sebastian S, Luban J. TRIM5alpha selectively binds a restriction-sensitive retroviral capsid. Retrovirology 2005;2:40.

[11] Stremlau M, Perron M, Lee M, Li Y, Song B, Javanbakht H, et al. Specific recognition and accelerated uncoating of retroviral capsids by the TRIM5alpha restriction factor. Proc Natl Acad Sci U S A 2006;103:5514–9.

[12] Yang H, Ji X, Zhao G, Ning J, Zhao Q, Aiken C, et al. Structural insight into HIV-1 capsid recognition by rhesus TRIM5α. Proc Natl Acad Sci U S A 2012;109:18372–7.

[13] Hatziioannou T, Evans DT. Animal models for HIV/AIDS research. Nat Rev Microbiol 2012;10:852–67.

[14] Nomaguchi M, Doi N, Fujiwara S, Adachi A. Macaque-tropic HIV-1 derivatives: a novel experimental approach to understand viral replication and evolution in vivo. In: Chang Theresa Li-Yun, editor. HIV-host interactions; 2011. p. 325–48. InTech, Rijeka, Croatia, http://www.intechopen.com/books/hiv-host-interactions/macaque-tropic-hiv-1-derivatives-a-novel-experimental-approach-to-understand-viral-replication-and-e.

[15] Nomaguchi M, Yokoyama M, Kono K, Nakayama EE, Shioda T, Doi N, et al. Generation of rhesus macaque-tropic HIV-1 clones that are resistant to major anti-HIV-1 restriction factors. J Virol 2013;87:11447–61.

[16] Soll SJ, Wilson SJ, Kutluay SB, Hatziioannou T, Bieniasz PD. Assisted evolution enables HIV-1 to overcome a high TRIM5α-imposed genetic barrier to rhesus macaque tropism. PLoS Pathog 2013;9:e1003667.

[17] Hatziioannou T, Princiotta M, Piatak Jr M, Yuan F, Zhang F, Lifson JD, et al. Generation of simian-tropic HIV-1 by restriction factor evasion. Science 2006;314:95.

[18] Kono K, Song H, Yokoyama M, Sato H, Shioda T, Nakayama EE. Multiple sites in the N-terminal half of simian immunodeficiency virus capsid protein contribute to evasion from rhesus monkey TRIM5α-mediated restriction. Retrovirology 2010;7:72.

[19] O'Doherty U, Swiggard WJ, Malim MH. Human immunodeficiency virus type 1 spinoculation enhances infection through virus binding. J Virol 2004;74:10074–80.

[20] Bichel K, Price AJ, Schaller T, Towers GJ, Freund SM, James LC. HIV-1 capsid undergoes coupled binding and isomerization by the nuclear pore protein NUP358. Retrovirology 2013;10:81.

[21] Hatziioannou T, Cowan S, Von Schwedler UK, Sundquist WI, Bieniasz PD. Species-specific tropism determinants in the human immunodeficiency virus type 1 capsid. J Virol 2004;78:6005–12.

[22] Kamada K, Igarashi T, Martin MA, Khamsri B, Hatcho K, Yamashita T, et al. Generation of HIV-1 derivatives that productively infect macaque monkey lymphoid cells. Proc Natl Acad Sci U S A 2006;103:16959–64.

[23] Kuroishi A, Saito A, Shingai Y, Shioda T, Nomaguchi M, Adachi A, et al. Modification of a loop sequence between alpha-helices 6 and 7 of virus capsid (CA) protein in a human immunodeficiency virus type 1 (HIV-1) derivative that has simian immunodeficiency virus (SIVmac239) vif and CA alpha-helices 4 and 5 loop improves replication in cynomolgus monkey cells. Retrovirology 2009;6:70.

[24] Lin TY, Emerman M. Determinants of cyclophilin A-dependent TRIM5 alpha restriction against HIV-1. Virology 2008;379:335–41.

[25] McCarthy KR, Schmidt AG, Kirmaier A, Wyand AL, Newman RM, Johnson WE. Gain-of-sensitivity mutations in a Trim5-resistant primary isolate of pathogenic SIV identify two independent conserved determinants of Trim5α specificity. PLoS Pathog 2013;9:e1003352.

[26] Nomaguchi M, Yokoyama M, Kono K, Nakayama EE, Shioda T, Saito A, et al. Gag-CA Q110D mutation elicits TRIM5-independent enhancement of HIV-1mt replication in macaque cells. Microbes Infect 2013;15:56–65.

[27] Ohkura S, Goldstone DC, Yap MW, Holden-Dye K, Taylor IA, Stoye JP. Novel escape mutants suggest an extensive TRIM5α binding site spanning the entire outer surface of the murine leukemia virus capsid protein. PLoS Pathog 2011;7:e1002011.

[28] Owens CM, Song B, Perron MJ, Yang PC, Stremlau M, Sodroski J. Binding and susceptibility to postentry restriction factors in monkey cells are specified by distinct regions of the human immunodeficiency virus type 1 capsid. J Virol 2004;78:5423–37.

[29] Pacheco B, Finzi A, Stremlau M, Sodroski J. Adaptation of HIV-1 to cells expressing rhesus monkey TRIM5α. Virology 2010;408:204–12.

[30] Kirmaier A, Wu F, Newman RM, Hall LR, Morgan JS, O'Connor S, et al. TRIM5 suppresses cross-species transmission of a primate immunodeficiency virus and selects for emergence of resistant variants in the new species. PLoS Biol 2010;8:e1000462.

[31] Newman RM, Hall L, Connole M, Chen GL, Sato S, Yuste E, et al. Balancing selection and the evolution of functional polymorphism in Old World monkey TRIM5alpha. Proc Natl Acad Sci U S A 2006;103:19134–9.

[32] Wilson SJ, Webb BL, Ylinen LM, Verschoor E, Heeney JL, Towers GJ. Independent evolution of an antiviral TRIMCyp in rhesus macaques. Proc Natl Acad Sci U S A 2008;105:3557–62.

[33] Price AJ, Marzetta F, Lammers M, Ylinen LM, Schaller T, Wilson SJ, et al. Active site remodeling switches HIV specificity of antiretroviral TRIMCyp. Nat Struct Mol Biol 2009;16:1036–42.

[34] Ylinen LM, Price AJ, Rasaiyaah J, Hué S, Rose NJ, Marzetta F, et al. Conformational adaptation of Asian macaque TRIMCyp directs lineage specific antiviral activity. PLoS Pathog 2010;6:e1001062.
[35] Wu F, Kirmaier A, Goeken R, Ourmanov I, Hall L, Morgan JS, et al. TRIM5 alpha drives SIVsmm evolution in rhesus macaques. PLoS Pathog 2013;9:e1003577.
[36] Doi N, Fujiwara S, Adachi A, Nomaguchi M. Rhesus M1.3S cells suitable for biological evaluation of macaque-tropic HIV/SIV clones. Front Microbiol 2011;2:115.
[37] von Schwedler UK, Stray KM, Garrus JE, Sundquist WI. Functional surfaces of the human immunodeficiency virus type 1 capsid protein. J Virol 2003;77:5439–50.
[38] Nomaguchi M, Doi N, Fujiwara S, Saito A, Akari H, Nakayama EE, et al. Systemic biological analysis of the mutations in two distinct HIV-1mt genomes occurred during replication in macaque cells. Microbes Infect 2013;15:319–28.

PLOS | ONE

RESEARCH ARTICLE

The HIV-1 Gp120/CXCR4 Axis Promotes CCR7 Ligand-Dependent CD4 T Cell Migration: CCR7 Homo- and CCR7/CXCR4 Hetero-Oligomer Formation as a Possible Mechanism for Up-Regulation of Functional CCR7

Haruko Hayasaka[1]*, Daichi Kobayashi[1], Hiromi Yoshimura[1], Emi E. Nakayama[2], Tatsuo Shioda[2], Masayuki Miyasaka[3,4]

1 Laboratory of Immune Regulation, Department of Microbiology and Immunology, Graduate School of Medicine, WPI Immunology Frontier Research Center, Osaka University, Suita, Osaka, Japan, **2** Department of Viral Infections, Research Institute for Microbial Diseases, Osaka University, Suita, Osaka, Japan, **3** Institute for Academic Initiatives, Osaka University, Suita, Osaka, Japan, **4** MediCity Laboratory, University of Turku, Tykistökatu 6A, 20520, Turku, Finland

* hayasaka@orgctl.med.osaka-u.ac.jp

OPEN ACCESS

Citation: Hayasaka H, Kobayashi D, Yoshimura H, Nakayama EE, Shioda T, Miyasaka M (2015) The HIV-1 Gp120/CXCR4 Axis Promotes CCR7 Ligand-Dependent CD4 T Cell Migration: CCR7 Homo- and CCR7/CXCR4 Hetero-Oligomer Formation as a Possible Mechanism for Up-Regulation of Functional CCR7. PLoS ONE 10(2): e0117454. doi:10.1371/journal.pone.0117454

Academic Editor: Yuntao Wu, George Mason University, UNITED STATES

Received: July 29, 2014

Accepted: December 24, 2014

Published: February 17, 2015

Data Availability Statement: All relevant data are within the paper.

Funding: This work is supported by the Ministry of Education, Culture, Sports, Science and Technology (Grant-in-Aid for Scientific Research on Innovative Areas, 21121007 to HH). The funders had no role in study design, data collection and analysis, decision to publish, or preparation of the manuscript.

Abstract

During human immunodeficiency virus (HIV) infection, enhanced migration of infected cells to lymph nodes leads to efficient propagation of HIV-1. The selective chemokine receptors, including CXCR4 and CCR7, may play a role in this process, yet the viral factors regulating chemokine-dependent T cell migration remain relatively unclear. The functional cooperation between the CXCR4 ligand chemokine CXCL12 and the CCR7 ligand chemokines CCL19 and CCL21 enhances CCR7-dependent T cell motility *in vitro* as well as cell trafficking into the lymph nodes *in vivo*. In this study, we report that a recombinant form of a viral CXCR4 ligand, X4-tropic HIV-1 gp120, enhanced the CD4 T cell response to CCR7 ligands in a manner dependent on CXCR4 and CD4, and that this effect was recapitulated by HIV-1 virions. HIV-1 gp120 significantly enhanced CCR7-dependent CD4 T cell migration from the footpad of mice to the draining lymph nodes in *in vivo* transfer experiments. We also demonstrated that CXCR4 expression is required for stable CCR7 expression on the CD4 T cell surface, whereas CXCR4 signaling facilitated CCR7 ligand binding to the cell surface and increased the level of CCR7 homo- as well as CXCR4/CCR7 hetero-oligomers without affecting CCR7 expression levels. Our findings indicate that HIV-evoked CXCR4 signaling promotes CCR7-dependent CD4 T cell migration by up-regulating CCR7 function, which is likely to be induced by increased formation of CCR7 homo- and CXCR4/CCR7 hetero-oligomers on the surface of CD4 T cells.

Competing Interests: The authors have declared that no competing interests exist.

Introduction

The human immunodeficiency virus type 1 (HIV-1) infects cells by utilizing its major envelope protein gp120 that binds to CD4 and also to chemokine receptors on human cells. In the case of $CD4^+$ T cells, the HIV gp120 first binds to CD4 and then to CXCR4, which triggers fusion of viral and cellular membranes and confers virus entry to cells. The gp120/CD4/CXCR4 interaction also initiates various intracellular signaling pathways [1–4], which affect the migration patterns and activation status of target cells.

Under physiological conditions, recruitment of lymphocytes from the blood into the secondary lymphoid tissues is regulated by the interaction between lymphoid chemokines such as CCL19, CCL21, CXCL12, and CXCL13, and their specific G-protein-coupled receptors [5], [6]. CCL19 and CCL21 bind to a common receptor, CC-chemokine receptor 7 (CCR7) [7], [8], whereas CXCL12 acts on T and B cells through its specific receptor CXCR4 [9]. CXCL13 selectively interacts with CXCR5 in B cells [10], and mediates efficient B cell trafficking to Peyer's patches and lymph nodes (LNs) [11], [12]. These lymphoid chemokines are selectively localized on the luminal surface and basal lamina of specialized venules of LNs known as high endothelial venules (HEVs), and in the parenchyma of the LNs and spleen [13], where they are presented to the circulating lymphocytes expressing corresponding G-protein-coupled receptors. The chemokine/chemokine receptor interaction induces β_2 integrin activation, resulting in lymphocyte adhesion to HEV endothelial cells expressing selective adhesion molecules and subsequent cell migration across the HEV basal lamina [5], [6].

Although a single chemokine is able to bind to and activate its corresponding chemokine receptor(s), functional cooperation between different chemokines has also been reported in various cell types. CXCL13 promotes CCR7 ligand-dependent chemotaxis of peripheral blood lymphocytes [14], and CXCL12 and CCR5 ligand chemokines act cooperatively in chemokine-induced T cell costimulation [15]. It is also known that CXCR3 ligands [16] and CCR7 ligands act cooperatively with CXCL12 to enhance CXCR4 ligand-dependent plasmacytoid dendritic cell recruitment [17]. Previously, we reported that CXCL12 binding to CXCR4 enhanced CCR7 ligand-dependent chemotaxis and intracellular signaling events in T cells *in vitro* [18]. This enhancing effect of CXCL12 on CCR7 activity was also observed *in vivo*; CXCL12 promoted CCR7-dependent T cell binding to HEVs and their subsequent migration into the LN parenchyma [18]. Given that multiple lymphoid chemokines, including CXCL12 and CCR7 ligand chemokines, are closely localized on the luminal surface and/or the basal lamina of HEVs, it is tempting to speculate that the combinational effects of these chemokines might cause efficient and specific lymphocyte trafficking to the LNs and Peyer's patches.

Green et al. [19] implies that non-chemokine ligands may also act to promote chemokine-induced T cell migration. In particular, they observed that the CXCR4-tropic (X4) envelope glycoprotein gp120 of $HIV\text{-}1_{IIIB}$ promoted CD4 T cell responses to CCL21/CCR7 and CCL20/CCR6 as well as CD4 T cell accumulation in LNs. The promoting effect of HIV-1 on chemokine-dependent CD4 T cell migration raises the possibility that the gp120-CXCR4 interaction may enhance not only virus entry but also chemokine-dependent intracellular signaling and subsequent cell migration, thus contributing to rapid virus spread *in vivo*. However, the precise mechanism underlying the enhancing effects of gp120 on CCR7 and CCR6 responses as well as the actual involvement of CXCR4 or CCR7 in this process remain unclear.

In the current study, we examined the molecular mechanisms underlying the enhancing effect of gp120 on CCR7 responses using a recombinant $HIV_{NL4\text{-}3}$-derived gp120. We determined that the enhancing effect was dependent on CXCR4 and CD4, and that not only recombinant gp120 but also the whole HIV virions enhanced CD4 T cell responses to CCR7 ligands. In addition, we found that CXCR4 signaling facilitated CCR7 ligand binding to the cell

surface, thereby increasing the level of CCR7 homo- and CCR7/CXCR4 hetero-oligomers without affecting CCR7 expression levels. In the following sections, we will discuss the functional significance of gp120/CXCR4-induced CCR7 oligomer formation in the up-regulation of CCR7.

Materials and Methods

Antibodies and reagents

Functional-grade purified anti-human CXCR4 monoclonal antibody (mAb; clone 12G5) and anti-human CD4 mAb (RPA-T4) were purchased from eBioscience (San Diego, CA, USA). Anti-human CCR7 mAb (clone 150503), anti-human CCR1 mAb (clone 53504), recombinant human CXCL12/SDF-1α, recombinant human 6Ckine/CCL21, and recombinant soluble CD4 (sCD4) were purchased from R&D Systems (Minneapolis, MN, USA). The anti-HIV-1 gp120 mAb 902 was affinity purified from mouse ascites fluid. AMD3100 was purchased from Sigma-Aldrich (St. Louis, MO, USA). The virus-free and concentrated culture supernatant of CV1 cells infected with recombinant Sendai virus (SeV) expressing the envelope glycoprotein gp120 subunit derived from the HIV-1 X4 strain NL4-3, the virus-free and concentrated culture supernatant of CV1 cells infected with parental SeV, and affinity-purified HIV gp120 in elution buffer (80 mM acetic acid and 0.17 M Tris-HCl) were all prepared as previously described [20]. Wild-type and gp120-deficient HIV NL4-3 virions [21] were prepared from culture supernatants of the HIV-infected human T cell line MT4 and treated with aldrithiol-2 (AT-2) for 30 min at 37°C to inactivate their infectivity. Virus particles were concentrated through a 20% sucrose cushion by ultracentrifugation (120,000 × *g*, 2 h, 4°C) and resuspended in 10% fetal calf serum (FCS)/RPMI1640. Control samples were prepared from non-infected MT4 cells.

Cells

Human peripheral blood mononuclear cells were obtained from healthy donors under written informed consent. Use of human materials in this study was approved by the Research Ethics Committee of Osaka University. Mononuclear cells were obtained by using Lymphoprep (Axis-Shield Diagnostics, Dundee, Scotland), according to manufacturer's instructions, and $CD4^+$ T cells were enriched using the $CD4^+$ T Cell Isolation Kit II (Miltenyi Biotec, Bergisch Gladbach, Germany). A human $CD4^+$ T cell line, H9 (HTB-176; obtained from American Type Culture Collection), was cultured in RPMI1640 supplemented with 10% (V/V) FCS, 2 mM L-glutamine, 1 mM sodium pyruvate, 100 U/ml penicillin, 100 μg/ml streptomycin, 50 μM 2-ME, 0.1 mM nonessential amino acids, and 10 mM HEPES.

Cell migration assay

A time-lapse cell migration assay was performed using an EZ-TAXIScan system (GE Healthcare Japan, Tokyo, Japan) as reported previously [18]. $CD4^+$ T cells (2×10^7/ml) were resuspended in 0.1% fatty acid-free bovine serum albumin (BSA)/FCS-free RPMI1640 medium, and were pretreated with the gp120 culture supernatant, control culture supernatant, recombinant gp120 (1 μg/ml), or elution buffer for 30 min at room temperature in the presence of anti-CCR7 mAb, anti-CXCR4 antibody, control mouse IgG, sCD4, or AMD3100. After pretreatment, the cell suspension was loaded into each well of the EZ-TAXIScan microchamber. After cell alignment was complete, human CCL21 (100 ng) was applied to the contra-wells. Cell migration was recorded along a concentration gradient of the chemokine over a horizontal glass surface under a silicon chip with a CCD camera at time-lapse intervals, and the digital images were analyzed. The total number of migrated cells that reached the fixed window, which was

located in the assay field two-thirds away from the starting point of cell migration, was counted, as described previously [22].

CD4 T cell chemotaxis was also analyzed by using a transwell-based double-chamber system with 3-μm pore-sized polycarbonate filters (ChemoTx) as described previously [18]. Briefly, purified human $CD4^+$ T cells (1×10^5 cells) were resuspended in 0.1% BSA/phenol red-free RPMI1640 medium, pretreated with the purified gp120 (5, 10, 20, or 40 μg/ml) or elution buffer for 30 min at room temperature, and were applied to the upper wells of a ChemoTx plate. CCL21 (250 or 1000 ng/ml) or vehicle control (phosphate-buffered saline, PBS) was applied to the lower wells. After 2 h incubation, the migrated cells were verified by the fluorometric determination of living cell numbers using a Cell Counting kit-F (Dojindo, Kumamoto, Japan). The fluorescence intensity was measured on a spectrofluorometer (SpectroMax; Molecular Devices, Sunnyvale, CA, USA).

Animals

All animal experiments were performed using protocols approved by the Ethics Review Committee for Animal Experimentation of Osaka University Graduate School of Medicine (approved number: 24–103). C57BL/6 (Japan SLC, Hamamatsu, Japan) and *plt/plt* mice on the C57BL/6 background (provided by Dr. H. Nakano of the National Institute of Environmental Health Sciences, USA) were housed under specific pathogen-free conditions. All the injections were carried out under isoflurane anesthesia.

Whole mount analysis

Human CD4 T cells were labeled with 10 μM 5-(and-6)-carboxyfluorescein diacetate, succinimidyl ester (CFSE; Invitrogen, Carlsbad, CA, USA) for 10 min at 37°C, and resuspended in RPMI1640 with 10% FCS. The labeled cells (5×10^6 cells) were injected into the footpads of C57BL/6 or *plt/plt* mice. A sham operation (PBS injection) was performed on the contralateral side. Popliteal lymph nodes (pLNs) were harvested from recipient mice after the transfer and fixed with 4% paraformaldehyde, and then treated with 30% sucrose. The images of pLNs were analyzed by confocal microscopy (TCS SL or TCS SP5; Leica). The number of cells was counted by using the publicly available image analysis software Image J (National Institutes of Health, Bethesda, MD, USA).

Flow-cytometric analysis

H9 cells (2×10^6) were transfected with 20 pmol of CCR7, CXCR4, or control siRNA (Santa-Cruz, sc-39888, sc-35421, and sc-37007) using the Cell Line Nucleofector Kit R (Lonza, Basel, Switzerland), according to manufacturer's instructions. Cells were harvested 10 hrs after transfection, and subjected to flow cytometry using anti-CCR7, anti-CXCR4, anti-CCR1 mAb, or control immunoglobulin. The fluorescence intensity of the AlexaFluor 488-conjugated goat anti-mouse IgG (Invitrogen) staining was measured by a FACSVerse (BD Biosciences) and analyzed by FlowJo software (Tree Star Inc., Palo Alto, CA). Detection of the CCR7 expression levels after gp120 or CXCL12 pre-treatment was perfomed as follows. Human peripheral mononuclear cells or H9 cells were preincubated with or without 0.1% BSA with PBS, CXCL12 (100 ng/ml), or recombinant gp120 (1 μg/ml) for 30 min, and then stained with phycoerythrin-conjugated anti-CCR7 mAb or control immunoglobulin. Human peripheral mononuclear cells were stained in the presence of with allophycocyanin-conjugated anti-human CD4 mAb for gating on the $CD4^+$ cells. Each result shown is a representative result of three independent experiments.

Western blotting

Cell lysates were prepared in 50 mM Tris-HCl, 20 mM NaF, 1 mM Na_3VO_4, 1% $NaPO_4$, 2 mM EDTA, and 150 mM NaCl, with proteinase inhibitor cocktail (Sigma-Aldrich). The samples were separated by SDS-PAGE, transferred onto PVDF membranes for immunoblotting with a rabbit anti-CCR7 mAb (Abcam, Cambridge, MA, USA, clone Y59) and a biotin-coupled anti-rabbit IgG antibody (Merck Millipore, Darmstadt, Germany), and detected by using horseradish peroxidase (HRP)–conjugated streptavidin and the ECL system (GE Healthcare Japan). Anti-β actin mAb (Wako Pure Chemical Industries, Osaka, Japan, clone 2F3) and mouse anti-CCR7 mAb (clone 150503) were detected by a HRP-conjugated goat anti-mouse antibody (American Qualex, San Clemente, CA, USA).

Ligand binding assay

H9 cells were seeded on fibronectin-coated wells and treated with 0.1% BSA with PBS, CXCL12 (100 ng/ml), or recombinant gp120 (1 μg/ml) for 30 min. Binding of CCL19-Ig (1 μg/ml; eBioscience) to T cells was detected by staining with 5 μg/ml biotin-conjugated anti-human IgG (American Qualex) and 5 μg/ml Alexa Fluor 647-conjugated streptavidin (Invitrogen). The images were captured by a confocal microscope and analyzed with Duolink Image Tool software (Olink Bioscience, Uppsala, Sweden).

Proximity ligation assay

CCR7 homo-oligomer formation was examined by the Duolink proximity ligation assay (PLA; Olink Bioscience), in which oligomerized CCR7 appears as orange dots representing the presence of a protein-protein interaction complex. Briefly, H9 cells in culture media containing 0.1% BSA were treated with or without CXCL12 or recombinant gp120 in fibronectin-coated wells for 30 min, fixed with 4% paraformaldehyde, and stained with a 7.5 μg/ml anti-human CCR7 mAb (R&D, MAB197) independently conjugated with the complementary oligonucleotide probe generated by Duolink II Probemaker PLUS or MINUS (Olink Bioscience). CCR7/CXCR4 hetero-oligomerization was examined by using anti-human CCR7 and anti-human CXCR4 mAbs (eBioscience, clone 12G5), which were labeled with the PLA-Minus and the PLA-Plus probes, respectively. As a control, anti-human CCR1 mAb (R&D, clone 53504) was used. The complementary DNA strands in close proximity (<40 nm) were amplified using fluorescence, which were visualized using a confocal laser microscope. The images were analyzed using the Duolink Image Tool software (Olink Bioscience).

Results

The recombinant X4-tropic gp120 and a CCR7 ligand chemokine act synergistically on CD4 T cell migration

To examine the effect of recombinant gp120 on CCR7-dependent CD4 T cell migration, we evaluated the number of migrated T cells in response to CCL21 in the presence or absence of the recombinant HIV_{NL4-3}-derived gp120 in a real-time micro-chemotaxis chamber. CD4 T cells resuspended in the recombinant gp120-containing cell culture supernatant showed more efficient migration in the direction of the CCL21 gradient compared with those in the control (gp120-free) supernatant (Fig. 1A). By the end of the 3-h experimental period, the number of migrated CD4 T cells in the gp120 pretreatment group was approximately double that in the control treatment group (Fig. 1B). However, in the absence of CCL21, gp120 did not affect the number of migrating cells, indicating that CD4 T cell migration is largely dependent on CCL21 (Fig. 1B). These results support the previous study by Green et al. [19] who showed that

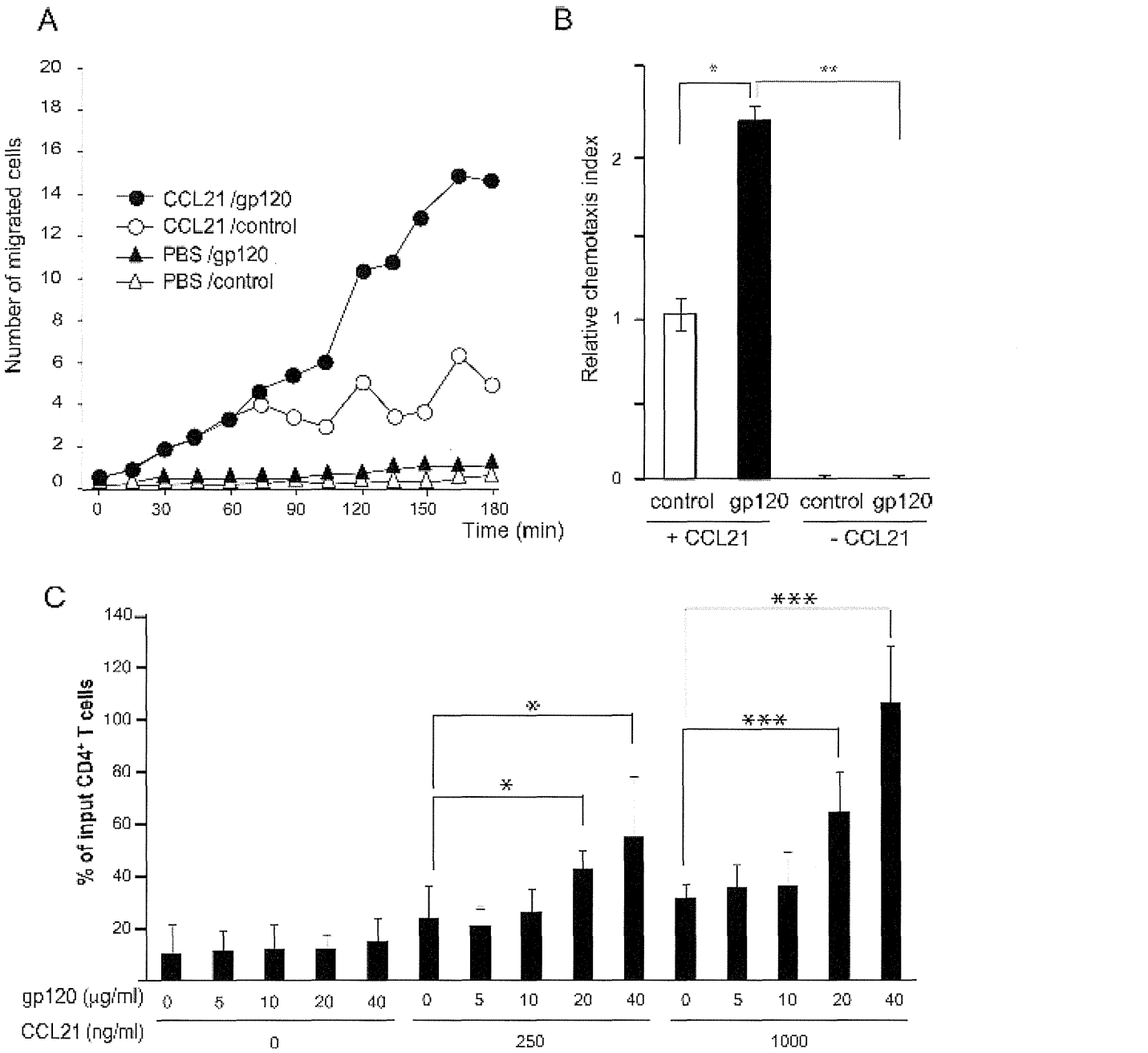

Fig 1. HIV-1_{NL4-3}-derived gp120 promoted CCL21-induced CD4 T cell chemotaxis. (A) Human CD4 T cells were incubated for 30 min at room temperature with the culture supernatant containing the recombinant HIV-1_{NL4-3}-derived gp120 (50 µg/ml, 420 nM) or a control solution, and chemotaxis in response to CCL21 was analyzed on a time-lapse video microscope. The number of cells in the fixed window, which was located in the assay field two-thirds away from the starting point of cell migration, was plotted against time after CCL21 injection. The result shown is a representative result of three independent experiments. (B) Quantification of the CCL21-induced CD4 T cell chemotaxis shown in panel A. The total number of migrated cells was calculated by summing the individual cell counts. The relative chemotaxis index represents the ratio of the number of migrated cells in the test treatment to that in control treatments (control solution in the presence of CCL21). Data represent means ± SEM of three independent experiments. *, $p < 0.05$ **, $p < 0.01$. (C) Human CD4 T cells (1×10^5) were mixed with the purified gp120 or control elution buffer and added to the upper wells of the transwell plate. The number of migrated cells in response to CCL21, which was added to the lower wells of the transwell plate, was analyzed. Graphs represent means ± SD percentage of input cells from triplicate wells. *, $p < 0.05$ ***, $p < 0.001$ by the Student's *t*-test.

doi:10.1371/journal.pone.0117454.g001

X4-tropic HIV-1_{IIIB}-derived gp120 enhances the responsiveness of CD4 T cells to CCR7 ligand chemokines.

We next examined the effect of purified recombinant HIV-1 gp120 on CD4 T cell migration in a transwell-based chamber assay (Fig. 1C). HIV-1 gp120 alone did not induce CD4 T cell migration at the concentrations examined in the absence of CCL21. In contrast, at concentrations of 20 μg/ml or higher, gp120 enhanced CD4 T cell migration at least 2-fold over the basal levels when 250 ng/ml or 1,000 ng/ml CCL21 was applied to the lower wells of the chamber. The enhancing effect of gp120 was dose-dependent, and was more prominent with an increase in CCL21 concentration, suggesting that gp120 and CCL21 cooperate synergistically on CD4 T cell migration.

HIV-1 gp120 promotes CCL21-induced CD4 T cell chemotaxis in a CXCR4- and CD4-dependent manner

To understand the mechanism underlying the enhancing effects of gp120 on CCR7 ligand-mediated responses, we examined its CXCR4 dependency. As expected, the number of migrated cells in response to CCL21 was significantly increased in the presence of HIV-1 gp120 and reduced to the basal level following application of a neutralizing anti-CCR7 antibody (Fig. 2A),

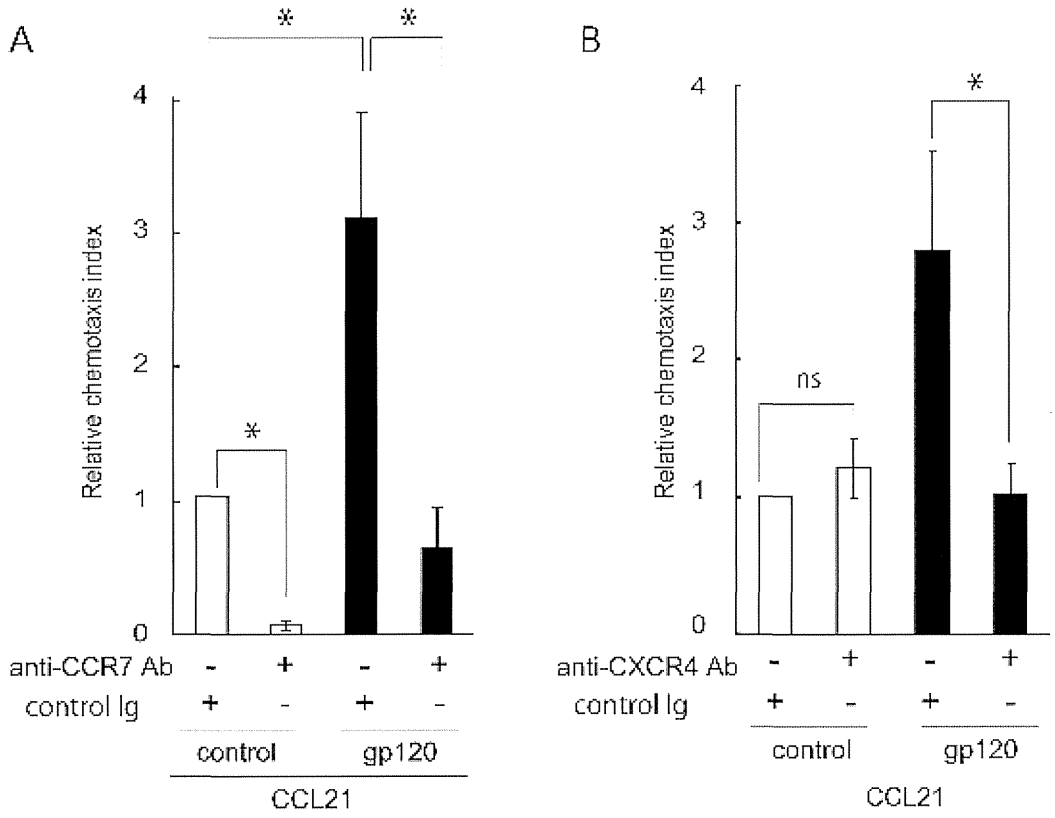

Fig 2. The effect of gp120 on CCL21-induced chemotaxis was dependent on CCR7 and CXCR4. (A) Human CD4 T cells were incubated for 30 min at room temperature with the culture supernatant containing recombinant gp120 (50 μg/ml) or a control solution, and chemotaxis in response to CCL21 was analyzed on a time-lapse video microscope. The total number of migrated cells was calculated by summing the individual cell counts. The assay was performed in the presence of a neutralizing anti-CCR7 antibody or control IgG (25 μg/ml). The relative chemotaxis index represents the ratio of the number of migrated cells in the test treatment to that in control treatments (control solution and control IgG). Data represent means ± SEM of three independent experiments. *, $p < 0.05$ by the Student's *t*-test. (B) The assay described above was performed in the presence of a neutralizing anti-CXCR4 antibody or control IgG. The relative chemotaxis index represents the ratio of the number of migrated cells in the test treatment to that in control treatments (control solution and control IgG).

doi:10.1371/journal.pone.0117454.g002

confirming its CCR7 dependency. In addition, CD4 T cell migration was also almost completely reduced to the basal level in the presence of an anti-CXCR4 neutralizing antibody (Fig. 2B) although the number of migrated cells was not altered in response to treatment of CCL21 alone, indicating that gp120 acts primarily through CXCR4 to enhance CCR7-dependent CD4 T cell chemotaxis.

It has been well established that HIV-1 gp120 forms a trimolecular complex with CD4 and CXCR4 in CD4 T cells [23]. We thus investigated the effect of a CXCR4 antagonist, AMD3100, and sCD4 on CCL21-induced migration using a CD4- and CXCR4-expressing H9 human T-lymphoma cell line; this cell line showed enhanced CCL21- or CCL19-dependent chemotaxis in the presence of gp120 at a comparable level to that observed in primary human CD4 T cells (data not shown). As shown in Fig. 3A, the enhancing effect of gp120 on CCL19-induced chemotaxis was significantly inhibited by AMD3100 or sCD4, as assessed in a real-time microchemotaxis chamber assay. In addition, in a transwell-based chamber assay, the effect of gp120 was inhibited, with cell numbers reaching almost basal levels, by a neutralizing anti-CXCR4 antibody, and was partially inhibited by sCD4 (Fig. 3B), confirming its dependency on CXCR4 and CD4.

HIV-1 virions promote CCR7-induced CD4 T cell migration

We next examined whether the native gp120 expressed on the viral envelope behaves in the same manner as recombinant gp120. As shown in Fig. 4A, whereas HIV-1 virion-containing

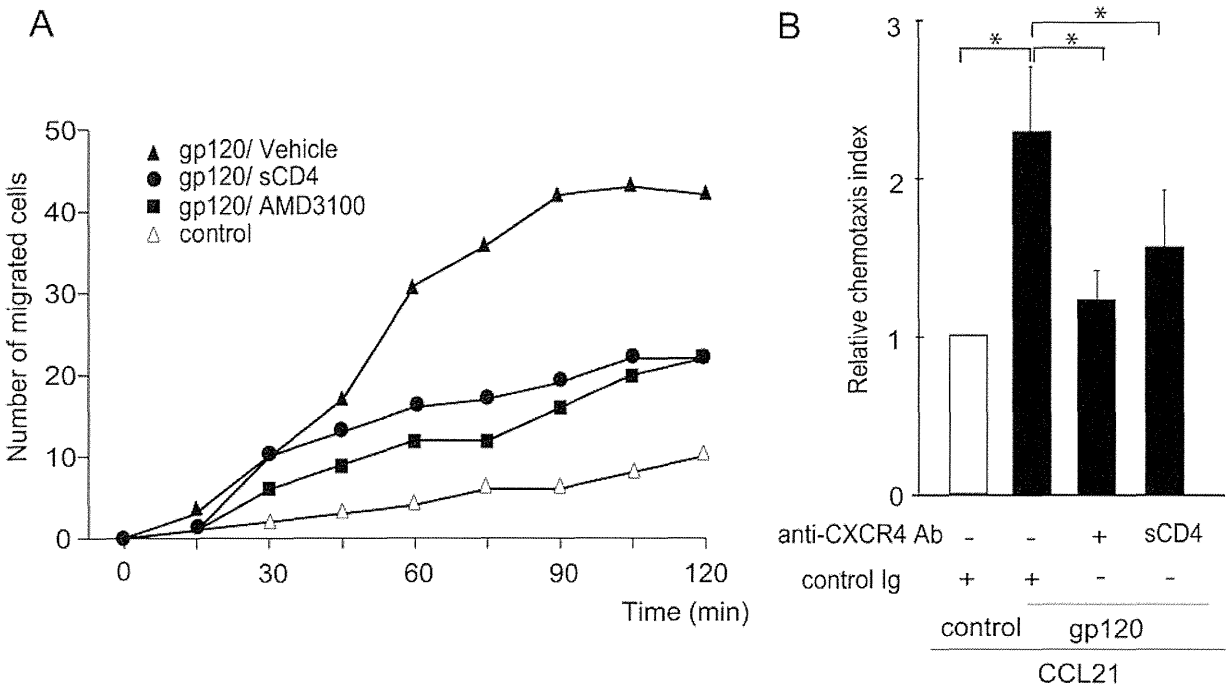

Fig 3. HIV-1 gp120 acted on CXCR4 and CD4 to promote CCR7-dependent human CD4 T cell migration. (A) CCR7 ligand-induced H9 cell migration after treatment with 1 μg/ml recombinant gp120 (filled symbols) or control buffer (open triangles) was examined on a time-lapse video microscope. CCL19-induced cell migration in H9 cells was examined in the presence of AMD3100 (25 μg/ml, filled squares), sCD4 (3 μg/ml, filled circles), or vehicle (filled triangles). The result shown is a representative result of three independent experiments. (B) CCR7 ligand-induced cell migration in the presence of a neutralizing anti-CXCR4 antibody, sCD4, or control IgG in H9 cells after treatment with 1 μg/ml recombinant gp120 (black bars) or control buffer (open bars). CCL21-induced cell migration was examined by a time-lapse video microscope, and the total number of migrated cells was calculated. The relative chemotaxis index represents the ratio of the number of migrated cells in the test treatment to that in control treatments (control solution in the presence of IgG). Data represent means ± SEM of three independent experiments. *, $p < 0.05$ by the Student's *t*-test.

doi:10.1371/journal.pone.0117454.g003

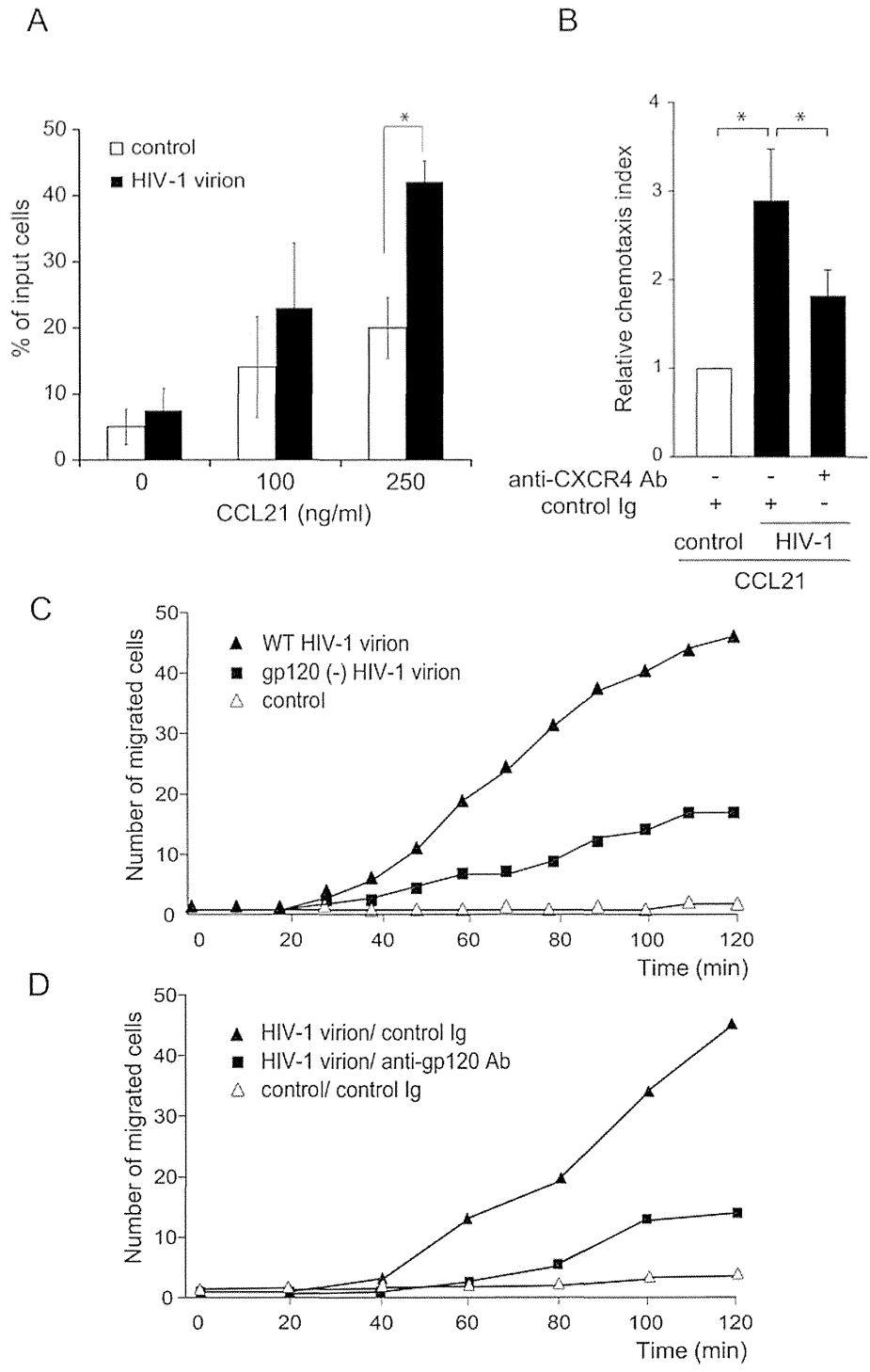

Fig 4. HIV-1 virions enhanced CCL21-induced CD4 T cell chemotaxis. (A) A CCR7 ligand-induced cell migration assay was performed using H9 cells (5×10^4) pre-treated with or without AT-2-inactivated HIV-1 virions (final concentration corresponding to 10 μg/ml p24) or control supernatant for 15 min. The number of migrated cells in response to CCL21 added to the lower wells of the transwell plate was analyzed. Graphs represent means ± SD percentage of input cells from triplicate wells. *, $p < 0.05$ by the Student's *t*-test. The result shown is a representative result of three independent experiments. (B) The time-lapse cell migration assay was performed in the presence of a neutralizing anti-CXCR4 antibody or control IgG. The relative chemotaxis index represents the ratio of the number of migrated cells in the test treatment to that in control treatments (control AT-2-treated mock supernatant in the presence of IgG). Data represent means ± SEM of

three independent experiments. *, $p < 0.05$ by the Student's *t*-test. (C) CCR7 ligand-induced H9 cell migration after treatment with AT-2-inactivated wild-type (WT) HIV-1 (filled triangles), gp120-deficient HIV-1 virions (filled squares) or control mock supernatant (open triangles). CCL19-induced cell migration was examined on a time-lapse video microscope. The result shown is a representative result of three independent experiments. (D) CCR7 ligand-induced H9 cell migration after treatment with AT-2-inactivated HIV-1 virions (filled symbols) or control supernatant (open triangles) in the presence of a neutralizing anti-gp120 antibody (50 μg/ml, filled squares) or control IgG (filled triangles). CCL21-induced cell migration was analyzed on a time-lapse video microscope. The result shown is a representative result of three independent experiments.

doi:10.1371/journal.pone.0117454.g004

culture media hardly affected the number of migrated cells in the absence of CCL21, cell migration was enhanced in the presence of CCL21 (250 ng/ml). A 2-fold increase in the number of migrated cells was observed in HIV-1 virion media compared with HIV-1-free culture media (Fig. 4A), and the enhancing effect was significantly inhibited in the presence of a neutralizing anti-CXCR4 antibody (Fig. 4B). The enhancing effect was significantly, albeit not completely, abrogated in a mutant HIV-1 lacking gp120 (Fig. 4C), indicating that at least a part of HIV-1 virion's effect is gp120-dependent. Supporting this result, the enhancing effect of HIV-1 virion was significantly inhibited by anti-gp120 neutralizing antibody (Fig. 4D). These results indicate that gp120 on the HIV viral envelope promotes CCR7-dependent CD4 T cell migration in a manner dependent on CXCR4.

HIV-1 gp120 promotes CCR7-dependent CD4 T cell trafficking to lymph nodes

Previously, Green et al. [19] reported that treatment of lymphocytes with gp120 from X4-tropic HIV_{IIIB} enhanced blood-borne lymphocyte migration to the LNs. In the present study, we investigated whether gp120 from X4-tropic HIV_{NL4-3} promotes lymph-borne T cell trafficking into lymphoid tissues in a manner dependent on CCR7. Given that lymphatic migration of T cells from the footpad to draining pLNs is CCR7-dependent and can be quantified by counting the number of migrating cells from the footpad to the pLN in the mouse [24], we first tested whether human T cells would migrate appropriately upon footpad injection in the mouse. After 2 h, injected T cells were observed in the pLN draining the injection side and their numbers gradually increased in a time-dependent manner (Fig. 5A), indicating that human T cells successfully migrated to the LNs via the lymphatic system of the mouse. At 15 h post injection, a large number of labeled CD4 T cells were observed in the pLN ipsilateral to the injected side but not in the contralateral pLN, confirming that mouse cells migrated into pLNs via the lymphatics but not via the blood vessels (comparable numbers of labeled cells would have appeared in ipsi- and contralateral pLNs if they had migrated via the blood vessels). Strikingly, when CCR7 ligand-deficient *plt/plt* mice were used as recipients, hardly any donor T cells appeared in the pLN even 15 h after injection (Fig. 5B), which further supports the hypothesis that their migration is CCR7-dependent. We then examined the effect of gp120. When human CD4 T cells were pretreated with purified recombinant gp120, they accumulated more efficiently in the pLN than those treated with control solution at time points examined (5, 15, 24 h) after footpad injection (Fig. 5C). The total number of migrated cells to the pLN was significantly higher in the gp120-treated group than that in the control group (Fig. 5D). In contrast, gp120-treated cell hardly migrated to the pLN *plt/plt* mice (data not shown). Collectively, these data support the notion that HIV gp120, in either the recombinant form or the native form expressed on the viral envelope, promotes lymphatic migration of CD4 T cells into peripheral LNs in a CCR7-dependent manner.

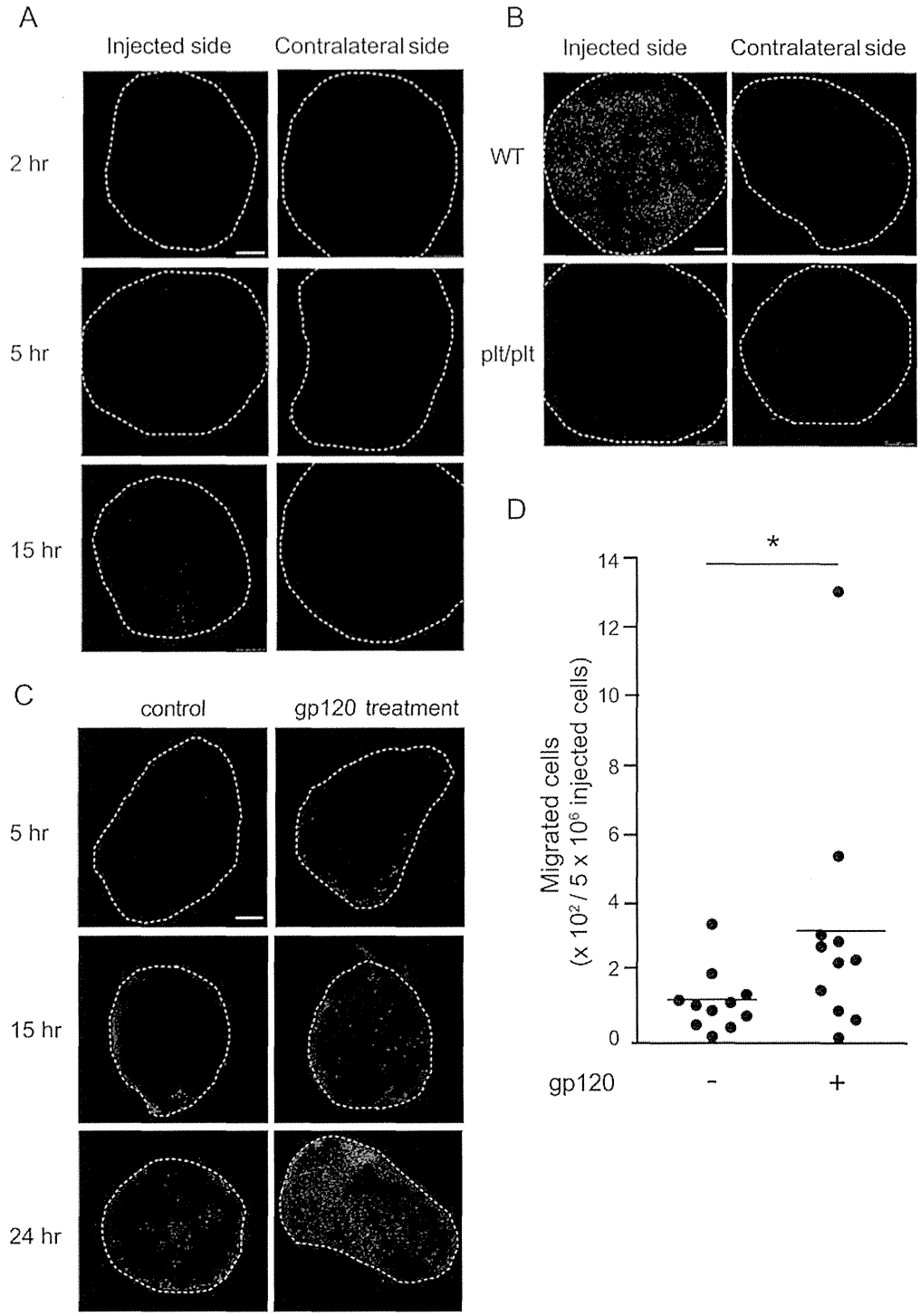

Fig 5. HIV-1 gp120 promoted CCR7-dependent CD4 T cell trafficking to the popliteal lymph nodes. (A) CFSE-labeled human CD4 T cells (5×10^6) were injected into the footpads of C57BL/6 WT mice. A sham operation (PBS injection) was performed on the contralateral side. Popliteal lymph nodes (pLNs) were harvested from the recipient mice at 2 h, 5 h, and 15 h after the transfer. (B) CFSE-labeled human CD4 T cells (5×10^6) were injected into the footpads of C57BL/6 WT mice or *plt/plt* mice. pLNs were harvested from the recipient mice at 15 h after cell transfer. The images of pLNs were analyzed by fluorescence confocal microscopy (original magnification ×100). Scale bar, 250 μm. (C) CFSE-labeled human CD4 T cells (5×10^6) were pretreated with purified gp120 (40 μg/ml) or control elution buffer, and injected into each side of C57BL/6 mouse footpad. pLNs were harvested from recipient mice at 5, 15, and 24 h after the transfer and analyzed by

confocal microscopy (TCS SP5; Leica). Representative images of pLNs obtained from 11 recipient mice subjected to CD4 T cell injection are shown. (D) The images obtained from individual mice (n = 11) at 5 h after the transfer were analyzed and the total numbers of migrated cells per 5×10^6 cells in a recipient mouse tissue was quantified using ImageJ software (NIH). *, $p < 0.05$ by the Wilcoxon signed-rank test.

doi:10.1371/journal.pone.0117454.g005

CXCR4 is required for stable CCR7 expression, and CXCR4 signaling promotes CCR7 ligand binding without affecting CCR7 expression

We next sought to determine the molecular mechanism by which CXCR4 signaling promotes CCR7-dependent CD4 T cell migration. To this end, we employed a small interfering RNA (siRNA) approach to suppress the cell surface expression of CXCR4 in CD4 T cells. We observed that CXCR4 siRNA selectively reduced CXCR4 expression by approximately three-fold (Fig. 6A, left). Interestingly, however, CXCR4 siRNA significantly diminished both the cell surface and total CCR7 expression in H9 cells (Fig. 6B). In contrast, CXCR4 siRNA did not reduce but rather slightly increased the cell surface CCR1 expression (Fig. 6A, right). This occurred without any changes in CCR7 expression at the mRNA level (Fig. 6C), supporting the hypothesis that CXCR4 expression contributes to stable CCR7 expression.

We then examined whether CXCR4 signaling affects CCR7 quantitatively or qualitatively. Preliminary experiments indicated that treatment with recombinant gp120 or CXCL12, at any of the concentrations that showed enhancing effects, did not alter CCR7 expression levels in human peripheral blood CD4 T cells and H9 cells (Fig. 6D). This result suggests that the enhancing effects of CXCR4 ligands on CCR7 signaling are not mediated by quantitative changes in CCR7 expression. We thus evaluated the ligand binding ability of CCR7 before and after CXCR4 ligation with CXCL12 or HIV gp120. As shown in Fig. 6E, gp120 or CXCL12 treatment increased the level of CCL19-Ig fusion protein binding to CD4 T cells by 3–5 times compared with mock treatment, in agreement with the hypothesis that CXCR4 signaling facilitates CCR7 ligand binding without affecting CCR7 expression levels, thus enhancing CCR7-mediated responses in CD4 T cells.

CXCR4 signaling promotes CCR7 homo- and CXCR4/CCR7 hetero-oligomerization

As receptor oligomerization is an important process for activating chemokine receptors [25], we next examined whether CXCR4 ligand binding affects CCR7 oligomerization on the surface of CD4 T cells. Using the *in situ* DuoLink PLA [26], we found that native gp120 significantly increased the signals generated by CCR7 homo-oligomers compared with a heat-denatured gp120 in CD4 T cells (Fig. 7A). Similarly to gp120, CXCL12 also increased CCR7 homo-oligomerization signals, and CXCL12's enhancing effect was inhibited by addition of a CXCR4 inhibitor, AMD3100, in a dose-dependent manner (Fig. 7B), indicating that the CXCL12-induced CCR7 homo-oligomerization is CXCR4-dependent.

Interestingly, CCR7 seemed to associate with not only CCR7 but also CXCR4, which appears to take place under constitutive conditions in CD4 T cells. Using the PLA, strong signals derived from CXCR4/CCR7 hetero-oligomers were observed even in the absence of CXCR4 or CCR7 ligands, whereas only very low signals were observed with CXCR4/CCR1 oligomers under the same conditions (Fig. 7C, D); CCR1 is a chemokine receptor expressed at a level comparable to that of CCR7 in H9 cells. These results indicate a basal association of CXCR4 with CCR7 on the surface of CD4 T cells. The basal CXCR4/CCR7 association appears to increase upon HIV gp120 binding to CXCR4. As shown in Fig. 7E, native HIV-1 gp120, but not its heat-denatured form, increased the level of CXCR4/CCR7 hetero-oligomerization by approximately two-fold. CXCL12 also showed an enhancing effect on CXCR4/CCR7 hetero-